17th IEEE International Conference on Smart Technologies

IEEE EUROCON 2017

6–8 July 2017, Ohrid, Macedonia

CONFERENCE PROCEEDINGS

Organized by:

IEEE Advancing Technology for Humanity

region 8 IEEE

IEEE Republic of Macedonia Section

Sponsored by:

netcetera

neotel

Part Number: CFP17EUR-ART

978-1-5090-3843-5

Conference Committees

Honorary Committee

Karen Bartleson,
2017 IEEE President,
Honorary Chair

Margaretha Eriksson,
IEEE R8 Director,
Honorary Co-Chair

Conference Steering Committee

Ljupco Karadzinov, Steering Committee Chair,
Ss. Cyril and Methodius University, Macedonia

Igor Kuzle, IEEE R8 Vice Chair for Technical Activities,
IEEE EUROCON 2013 General Chair,
University of Zagreb, Croatia

Peter Nagy, IEEE R8 Conference Coordination Subcommittee Chair (2017-2018),
Operations Director at Hírközlési és Informatikai Tudományos Egyesület, Hungary

Adel M. Alimi, IEEE R8 Conference Coordination Subcommittee Chair (2015-2016),
University of Sfax, Tunisia

Petar Popovski, Keynote Speaker, STA-1 Chair,
Aalborg University, Denmark

Liljana Gavrilovska, STA-2 Chair
Ss. Cyril and Methodius University, Macedonia

Andrzej Krawczyk, STA-3 Chair
Czestochowa University of Technology, Poland

Stephen Goodnick, Keynote Speaker, STA-4 Chair
Arizona State University, USA

Dragica Vasileska, STA-4 Co-Chair
Arizona State University, USA

Georgi Dimirovski, STA-5 Chair
Dogus University, Turkey and Ss. Cyril and Methodius University, Macedonia

Eckhard Grass, Keynote Speaker, STA-6 Chair
IHP - Leibniz-Institut für innovative Mikroelektronik and Humboldt-Universität zu Berlin, Germany

Yuanwei Jing, STA-7 Chair
Northeastern University, Shenyang, P. R. China

Jun Zhao, STA-8 Chair
Northeastern University, Shenyang, P. R. China

Alberto Tessarolo, STA-9 Chair
University of Trieste, Italy

Ahmed Zobaa, STA-10 Chair
Brunel University London, Uxbridge, United Kingdom

Bülent Ertan, STA-11 Chair
Middle East Technical University, Ankara, Turkey

Yuri Demchenko, STA-12 Chair
University of Amsterdam, Netherlands

Rafael Mihalič, Keynote Speaker, SS-1 Chair
University of Ljubljana, Slovenia

Technical Program Committee (TPC)

Goga Cvetkovski, TPC Chair,
Ss. Cyril and Methodius University, Macedonia

Muhammad Alam, Instituto de Telecomunicações, University of Aveiro, Portugal
Adel M. Alimi, University of Sfax, Tunisia
Francisco Arcega, University of Zaragoza, Spain
Pedro A. Amado Assuncao, Instituto Politecnico de Leiria/Instituto de Telecocomunicações, Portugal
Chitti Babu, The University of Nottingham (U.K) Malaysia Campus, Malaysia
Constantin Barbulescu, Politehnica University of Temisoara, Romania
Pavol Bauer, TU Delft, The Nederlands
João Catalão, University of Porto, Portugal
Owen Casha, University of Malta, Malta
Mihai Cernat, University of Translilvania, Romania
Mario Cifrek, University of Zagreb, Croatia
Snežana Čundeva, Ss. Cyril and Methodius University, Macedonia
Marko Čepin, University of Ljubljana, Slovenia
Anton Čauševski, Ss. Cyril and Methodius University, Macedonia
Carl James Debono, University of Malta, Malta
Vladimir Dimčev, Ss. Cyril and Methodius University, Macedonia
Georgi Dimirovski, Dogus University, Turkey & Ss. Cyril and Methodius University, Macedonia
Bulent Ertan, Middle East Technical University, Turkey
Francisco Falcone, Unicersity of Navara, Spain
Joaquim Ferreira, Instituto de Telecomunicações, University of Aveiro, Portugal
Sonja Filipovska, Ss. Cyril and Methodius University, Macedonia
José Fonseca, Instituto de Telecomunicações, University of Aveiro, Portugal
Liljana Gavrilovska, Ss. Cyril and Methodius University, Macedonia
Leonid Grcev, Macedonian Academy of Sciences and Arts, Skopje, Macedonia
Stephen Goodnick, Arizona State University, USA
Eckhard Grass, Universität zu Berlin, Germany
Sonia Haamstra de Groot, Technical University of Eindhoven, The Nederland
Miralem Hadžiselimović, University of Maribor, Slovenia
Andrej Gubina, University of Ljubljana, Slovenia
Yuanwei Jing, Northeastern University, P. R. China
Vladimir Katić, University of Novi Sad, Serbia
Slavko Krajcar, University of Zagreb, Croatia
Andrzej Krawczyk, Czestochowa University of Technology, Poland
Lukasz Kulas, Gdansk University of Technology, Poland
Igor Kuzle, University of Zagreb, Croatia
Paul Lefley, University of Leicester, United Kingdom
Emil Levi, Liverpool John Moores University, United Kingdom
Marin Marinov, Technical University of Sofia, Bulgaria
Vera Marković, University of Niš, Serbia

João Matos, Institute of Telecomunications - Polo de Aveiro, Portugal
Mário Rui Melicio da Conceição, University of Lisabon, Portugal
Rafael Mihalič, University of Ljubljana, Slovenia
Anastas Mishev, Ss. Cyril and Methodius University, Skopje, Macedonia
Jürgen Mottok, OTH Regensburg, Germany
Petre-Marian Nicolae, University of Craiova, Romania
Krzysztof Nyka, Gdansk University of Technology, Poland
Miloš Oravec, Slovak University of Technolgoy, Slovakia
Maria-Alexandra Paun, EPFL, Switzerland
Ljupco Pejov, Ss. Cyril and Methodius University, Skopje, Macedonia
Predrag Pejović, University of Belgrade, Serbia
Marjan Popov, Technical University of Delft, Netherlands
Petar Popovski, Aalborg University, Denmark
Tomáš Potužák, University of West Bohemia, Czech Republic
Katerina Raleva, Ss. Cyril and Methodius University, Macedonia
Meliha B. Selak, Power System Consultants, Canada
Ciprian Sorandaru, Politehnica University of Timisoara, Romania
Georgi Stojanov, American University of Paris, France
Georgi Stoyanov, Technical University in Sofia, Bulgaria
Bojan Štumberger, University of Maribor, Slovenia
Alberto Tessarolo, University of Trieste, Italy
Mirko Todorovski, Ss. Cyril and Methodius University, Macedonia
Abdellah Touhafi, Vrije Universiteit Brussel, Belgium
Dragica Vasileska, Arizona State University, USA
Stanimir Valtchev, University of Lisabon, Portugal
Peter Virtič, University of Maribor, Slovenia
Vladimir Vujičić, University of Novi Sad, Serbia
Tianhua Xu, University College London, United Kingdom
Damir Žarko, University of Zagreb, Croatia
Matej Zajc, University of Ljubljana, Slovenia
Saviour Zammit, University of Malta, Malta
Jun Zhao, Northeastern University, P. R. China
Ahmed Zobaa, Brunel University London, Uxbridge, United Kingdom
Jim Zou, ADVA Optical Networking SE, Germany

Power Control in Series-Resonant Bridge Inverters

Ljupco Karadzinov
Faculty of Electrical Engineering and IT
Sts. Cyril and Methodius University
Skopje, Republic of Macedonia
l.karadzinov@feit.ukim.edu.mk

Goce Stefanov
Faculty of Electrical Engineering
University Goce Delcev
Stip, Republic of Macedonia
goce.stefanov@ugd.edu.mk

***Abstract*—Direct phase or indirect frequency control methods are used in series-resonant bridge power inverters for induction heating to maintain maximum power transfer as the load equivalent electrical parameters change during the heating process. In these applications, to control the power level it is common to use the above resonance operating frequency, where only measurement of the deviation of the phase angle from its reference value is used to calculate the new bridge switching frequency. Below resonance is not used since its control is non-linear, has high level of harmonics and is considered unstable, so no detailed analysis have been carried out. The paper present mathematical analysis of the output power, voltage and current phase angle dependence on the resonant circuit damping frequency when it is excited with pulse voltage with a different frequency than the resonant one, in both above and below resonance regions. Based on this analysis, possibilities of below resonance power control are investigated and new insight in circuit behavior is presented based on variation in resonant tank parameter values.**

Keywords—series-resonant bridge inverter; direct phase control method; below resonance operating mode; damping frequency.

I. INTRODUCTION

Series-resonant bridge inverters are used in a variety of applications. Maximum energy is transferred to the load when the converter switching frequency is same to the resonant one. In some applications, like direct induction heating, the heated work-piece equivalent electrical parameters are part of the resonant circuit [1–4]. As the temperature of the work-piece is increased, the resonant tank inductance and resistance change, thus changing the circuit resonant frequency. To ensure maximum energy transfer, the inverter control circuitry must adjust the switching frequency so that it follows the change of the resonant frequency. Different control algorithms are used to adjust the switching to the resonant frequency. Several of them are based on direct frequency control [5–6] and other use indirect frequency control by controlling the phase angle φ between the inverter output voltage and current [7–15]. The last control type, instead of indirect frequency, is more often called direct phase control method. Phase control provides reliable drive of the resonant converter in the presence of large dynamic changes in the load impedance during star-up, natural tracking of component variations with temperature and time, simplified control to output dynamics and a more linear relationship between phase command and output current when compared to frequency control [10, 11].

In the analysis of serial resonant converters it is usual to use the resonant circuit frequency ω_0 for two reasons: (1) assuming that the value of the resistance of the resonant tank is very small the damping is negligible and thus resonant ω_0 and damping ω_d angular frequencies have very close values; (2) active power is calculated using the phase angle between voltage and current first harmonics. However, in resonant converters the voltage waveforms are pulse and current has a damped sinusoidal form. In such cases phase angle has to be calculated in respect to the damping frequency and consequently the derived expressions [16] show qualitatively different behavior. Based on damping frequency analysis of the dependence of the phase angle φ on the switching frequency ω_s in [16] improved direct phase control method was developed.

Applications in [10, 11, 16] use the above resonance operating mode. Below resonance operation mode (although it allows for zero current transistor switch-off and diode switch-on) is not used since has higher current distortion and lower power factor. Consequently, no detailed analytical investigations of this operation mode have been carried out and conclusion are derived form the usual harmonic analysis. In this paper equations are derived that are valid for the whole range of frequencies, below and above the resonance. They allow for further investigations of all parameters and power control in above and below resonance modes in series-resonant bridge inverters.

II. DIRECT PHASE CONTROL METHOD

Fig. 1 shows a block diagram of the feedback control circuitry used in the direct phase control of full-bridge series-resonant inverter. It comprises of a current transformer that measures the resonant circuit (output) current, a zero crossing detector that gives zero voltage when $i_{out}(t) < 0$ and positive voltage when $i_{out}(t) > 0$, a microcontroller that implements the control algorithm, optocoupler galvanic isolation, driver circuit that supplies firing pulses to the IGBT switches and feedback circuit for IGBT overload protection measuring collector-emitter voltages v_{CE} to limit currents through T1 to T4.

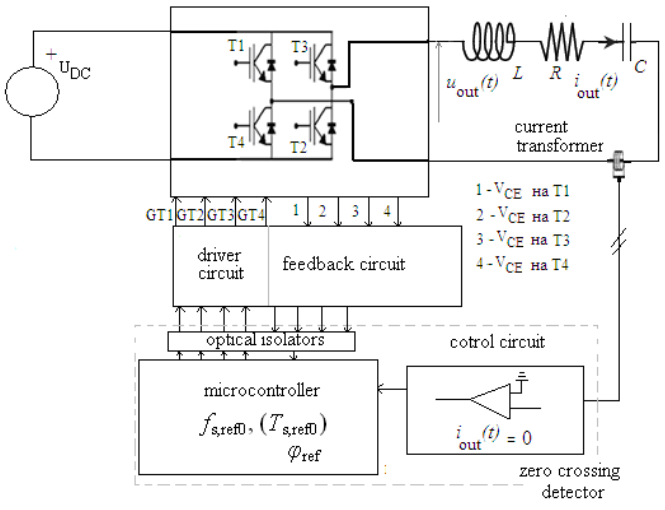

Fig. 1. Block diagram of the full-bridge series-resonant inverter.

978-1-5090-3843-5/17/$31.00 ©2017 IEEE

The microcontroller program has predefined values for the initial value of the switching frequency $f_{s,ref0}$ (or period $T_{s,ref0} = 1/f_{s,ref0}$) and the desired or the reference phase difference between the output voltage and current φ_{ref}. This phase difference would be zero or close to zero if maximum power transfer is needed, or have a specific value that corresponds to the desired output power when we like to control the power transfer.

Fig. 2 shows the output voltage and current waveforms in the more usual above-resonance mode of operation. In induction heating/melting and similar applications the heated work-piece equivalent electrical parameters are part of the resonant circuit. As the work-piece temperature increases, its equivalent resistance and inductance change, thus changing the circuit resonant frequency. Consequently, the deviation of the switching frequency from the resonant one is also changed, which results in undesired change of output power. The prototype resonant inverter for induction heating with rated power of 10 kW built in [16] has the resonant tank parameters $R = 0.24\ \Omega$, $L = 26.5\ \mu H$ and $C = 26.6\ \mu F$. The typical R and L change during metal-piece induction melting is in the range of ±50%. These real values are used as an example in the following investigation giving the values for the resonant frequency $\omega_0 = 37{,}665$ rad/s, $f_0 = 5{,}998$ Hz and the base value of the quality factor $Q = 4$ (more precisely 4.16) and its range from 3 to 5.

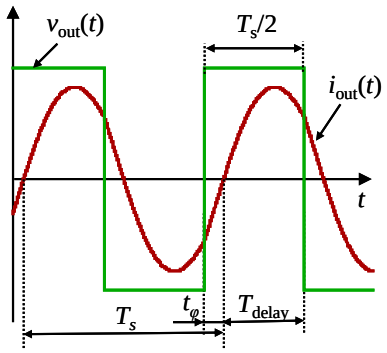

Fig. 2. Output voltage and current waveforms in above-resonance mode.

To maintain the desired output power the switching frequency needs to be adjusted. Control methods [10, 11, 16] achieve this by adjusting the interval T_{delay} (after which T3 and T4 are switched off, and T1 and T2 switched on) using an algorithm with 8 steps:

1. Switch-off T1 and T2, and switch-on T3 and T4, (positive half-period starts);
2. Wait for current zero crossing moment $i(t) > 0$ and measure time interval $t_{\varphi,i}$;
3. Calculate $T_{delay,i}$ using the method equations;
4. Wait for time interval $T_{delay,i}$;
5. Switch-on T1 and T2, and switch-off T3 and T4 (negative half-period starts);
6. Wait for current zero crossing moment $i(t) < 0$ and measure time interval $t_{\varphi,i}$;
7. Calculate $T_{delay,i}$;
8. Wait for time interval $T_{delay,i}$ and go to step 1.

The new values of the positive half-period and consequently the new switching frequency are determined by the desired phase angle which makes this method a direct phase control one. This method has an advantage of being very simple and easy to implement with a low cost microcontroller. The calculations in steps 3 (and 7) should be finished numerically before the positive half-period ends, i.e. during T_{delay} time. Having in mind that $T_s/2$ is less than 100 μs and t_φ in the order of 10 μs, the methods use simplified equations, so that the calculations can be done on a low cost microcontroller.

The main objective of the control method is to adjust the switching frequency so that the desired phase angle and power transfer are obtained. To do so, the feedback circuit in Fig. 1 has possibilities to measure the time between current zero crossings and instants when the switches are turned on or off. This means that the control method as input has the values of the previous cycle switching period $T_{s,i-1}$ and the current cycle phase angle time equivalent $t_{\varphi,i}$. Having these measured values, the method determines the new switching frequency $T_{s,i}$ at which the φ_i and $t_{\varphi,i}$ have the desired or the reference values.

III. SQUARE PULSE EXCITATION OF THE RESONANT TANK

Analysis of the series-resonant converters usually use the voltage and current first harmonics to determine the circuit parameters and behavior. However, the current waveform in Fig. 2 is not sine wave, but is comprised of pieces of damped oscillation and φ and t_φ depend on the circuit damping frequency ω_d. To derive the phase angle φ dependence on ω_d let us explore the series-resonant circuit excited by voltage pulses.

If the voltage is in form of the Heaviside step function, then the current oscillates around zero with angular damping frequency ω_d, as shown in Fig. 3. When the voltage has square pulses waveform (duty ratio $D = 0.5$) and amplitude $\pm V_{DC}$, then in every half-period the current is a piece of the damped oscillation of Fig. 3 and looks like the waveform shown in Fig. 2. In the steady state the negative half-period waveform is symmetrical to the positive one in respect to the time axis. Harmonic analysis can be done in this case for the calculation of the active and reactive power, power factor etc. However, to determine the t_φ (and φ) as defined in Fig. 2 and its dependence on the deviation of ω_s from ω_d, the actual time waveforms from Fig. 3 have to be analyzed. Such analysis has not been carried in the literature to the best of our knowledge.

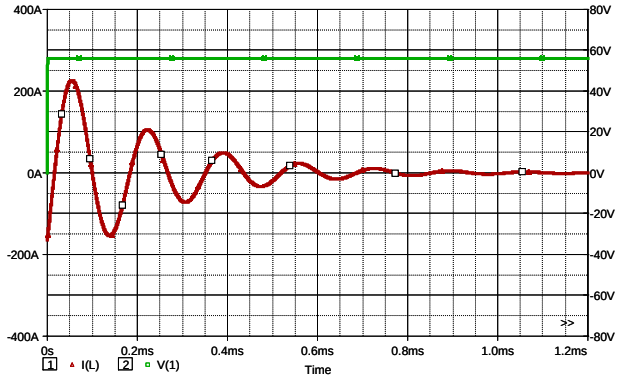

Fig. 3. Current waveform in the series-resonant circuit when excited by a Heaviside step voltage with amplitude $V_{DC} = 56$ V. Parameters' values are $R = 0.24\ \Omega$, $L = 26.5\ \mu H$ and $C = 26.6\ \mu F$ with initial values $i_L(0^+) = -165$ A and $u_C(0^+) = -163$ V to match the initial conditions in Fig. 2.

The series-resonant circuit current waveform for one half-period can be obtained from the second-order differential equation:

$$\frac{d^2 i(t)}{dt^2} + \frac{R}{L}\frac{di(t)}{dt} + \frac{i(t)}{CL} = \frac{1}{L}\frac{dv(t)}{dt} \qquad (3)$$

The solution in this case (using prototype real parameters) is the under-damped one ($\alpha < \omega_0$), which is also obvious since the current oscillates (Fig. 3), it has no DC component since $v(t)$ is constant ($dv/dt = 0$) and has the form (1) or (2):

$$i(t) = e^{-\alpha t}(A_1 \cos \omega_d t + A_2 \sin \omega_d t) \qquad (1)$$

$$i(t) = I_{max} e^{-\alpha t} \sin(\omega_d t - \varphi) \qquad (2)$$

where $\alpha = \frac{R}{2L} = 4528\text{s}^{-1}$, $\omega_0 = \frac{1}{\sqrt{LC}} = 37665\frac{\text{rad}}{\text{s}}$,

$\omega_d{}^2 + \alpha^2 = \omega_0^2 \Rightarrow \omega_d = \sqrt{\omega_0^2 - \alpha^2} = 37392\frac{\text{rad}}{\text{s}}$, and

$$Q = \frac{\omega_0 L}{R} = \frac{1}{\omega_0 RC} = \frac{1}{R}\sqrt{\frac{L}{C}} = \frac{\omega_0}{2\alpha} = 4.16 \quad (3)$$

Determination of the two unknown constants I_{max} and φ for the steady-state solution can be done using two border conditions for this time interval, i.e. $i(0) = -I_0$ and $i(T_s/2) = +I_0$:

for $t = 0$ $$i(0) = I_{max}\sin(-\varphi) = -I_0 \quad (4)$$

for $t = T_s/2$ $$i(\frac{T_s}{2}) = I_{max}e^{-\alpha\frac{T_s}{2}}\sin(\omega_d\frac{T_s}{2} - \varphi) = +I_0 \quad (5)$$

$$(5)\rightarrow I_{max}e^{-\alpha\frac{T_s}{2}}[\sin(\omega_d\frac{T_s}{2})\cos(-\varphi) + \cos(\omega_d\frac{T_s}{2})\sin(-\varphi)] = +I_0 \quad (6)$$

Dividing (6) by (4) we obtain:

$$\frac{e^{-\frac{\pi}{2Q}\frac{\omega_0}{\omega_s}}[\sin(\pi\frac{\omega_d}{\omega_s})\cos(-\varphi) + \cos(\pi\frac{\omega_d}{\omega_s})\sin(-\varphi)]}{\sin(-\varphi)} = -1$$

$$e^{-\frac{\pi}{2Q}\frac{\omega_0}{\omega_s}}[\frac{\sin(\pi\frac{\omega_d}{\omega_s})}{\tan(\varphi)} - \cos(\pi\frac{\omega_d}{\omega_s})] = 1$$

and finally: $$\varphi = \arctan\left(\frac{\sin(\pi\frac{\omega_d}{\omega_s})}{e^{+\frac{\pi}{2Q}\frac{\omega_0}{\omega_d}\frac{\omega_d}{\omega_s}} + \cos(\pi\frac{\omega_d}{\omega_s})}\right) \quad (7)$$

To determine the second unknown I_{max}, the inductor voltage border conditions can be used. The inductor voltage $v_L(t)$ obtained as derivative of its current $L\cdot$d$i(t)$/dt is given by:

$$v_L(t) = -LI_{max}e^{-\alpha t}[\alpha\sin(\omega_d t - \varphi) - \omega_d\cos(\omega_d t - \varphi)]$$

or representing it as single sine function with phase shift and using (3) the $v_L(t)$ has the form:

$$v_L(t) = -\omega_0 LI_{max}e^{-\alpha t}[\sin(\omega_d t - \varphi - \arctan(\frac{\omega_d}{\alpha})] \quad (8)$$

At the $t = 0^+$ using (8) we have:

$$v_L(0) = V_{L0} = -\omega_0 LI_{max}\sin(-\varphi - \arctan(\frac{\omega_d}{\alpha}) \quad (9)$$

At the end of positive half period $t = T^-/2$ using (8) we have:

$$v_L\left(\frac{T^-}{2}\right) = -\omega_0 LI_{max}e^{-\frac{\alpha}{\omega_d}\frac{\pi}{x}}\sin[\frac{\pi}{x} - \varphi - \arctan(\frac{\omega_d}{\alpha})] \quad (10)$$

When input voltage changes from V_{DC} to $-V_{DC}$, the resonant tank current $i(t)$, which is also inductor current, cannot have abrupt change. The same is the case with the resistor voltage $v_R(t) = R\cdot i(t)$ and the capacitor voltage $v_C(t)$. The whole change of $-2\cdot V_{DC}$ will appear in the inductor voltage:

$$v_L\left(\frac{T^+}{2}\right) = v_L\left(\frac{T^-}{2}\right) - 2V_{DC} \quad (11)$$

At the end of T/2 period the $v_L(t)$ has the same value as V_{L0}, but with an opposite sign:

$$v_L\left(\frac{T^+}{2}\right) = -V_{L0} \quad (12)$$

Combining (11) and (12):

$$v_L\left(\frac{T^-}{2}\right) = -V_{L0} + 2V_{DC} \quad (13)$$

Now using (9) and (10) in (13), one equation with one unknown I_{max} is obtained:

$$-\omega_0 LI_{max}e^{-\frac{\alpha}{\omega_d}\frac{\pi}{x}}\sin[\frac{\pi}{x} - \varphi - \arctan(\frac{\omega_d}{\alpha})] =$$

$$= \omega_0 LI_{max}\sin(-\varphi - \arctan(\frac{\omega_d}{\alpha}) + 2V_{DC}$$

Finally:

$$I_{max} = \frac{-\frac{2V_{DC}}{\omega_0 L}}{\sin[-\varphi - \arctan(\frac{\omega_d}{\alpha})] + e^{-\frac{\alpha}{\omega_d}\frac{\pi}{x}}\sin[\frac{\pi}{x} - \varphi - \arctan(\frac{\omega_d}{\alpha})]} \quad (14)$$

The resistor voltage is given by:

$$v_R(t) = Ri(t) = RI_{max}e^{-\alpha t}\sin(\omega_d t - \varphi) \quad (15)$$

The capacitor voltage $v_C(t)$, instead of being obtained as integral of its current, can be obtained as:

$$v_C(t) = v_{IN}(t) - v_R(t) - v_L(t) \quad (16)$$

Equations (2), (8), (15) and (16), together with parameters equations (7) and (14), give the exact analytical forms of all resonant tank time variables.

IV. SINE WAVE AND SQUARE PULSE EXCITATION COMPARISON

Before obtaining the expressions and analyzing the output power, lets comment on the difference in the two approaches, the sine-wave voltage exaction and the square-pulse excitation analysis cases. The difference is especially notable in the below resonance region.

When a series resonant circuit is excited by a sine wave voltage, all waveforms have the sine shape and the current phase φ in respect to the voltage is a well known relation:

$$\varphi = \text{arctg}[Q(\frac{\omega_s}{\omega_0} - \frac{\omega_0}{\omega_s})] \quad (17)$$

where ω_s is the operating, ω_0 the resonant angular frequency and the quality factor is Q. This monotonous relation is shown in Fig. 4 for the base value $Q = 4$ and its range from 3 to 5.

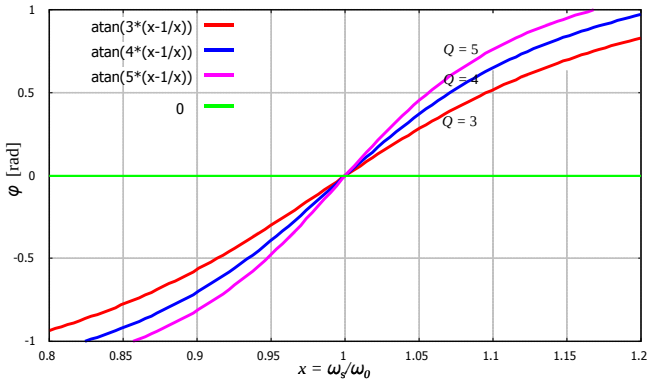

Fig. 4. Phase angle φ dependence on $x = \omega_s/\omega_0$ for $Q = 3$, 4 and 5, when the series resonant circuit is exited by a sinusoidal voltage.

When the series-resonant circuit is excited by voltage pulses, the current phase φ in respect to the voltage is given by the relation (7). It is graphed in Fig. 5 for $Q = 3$, 4 and 5 and shows considerably different behavior than (17) and Fig. 4. The function is not monotonous and it "oscillates" below resonance ($x = \omega_s/\omega_d < 1$) having negative, but also positive values for φ.

To visualize this rather strange dependence, Fig. 6 gives PSpice simulation results of steady-state for several values of the switching frequency below and above resonance. Phase angles measured in these waveforms match and verify results obtained by (7).

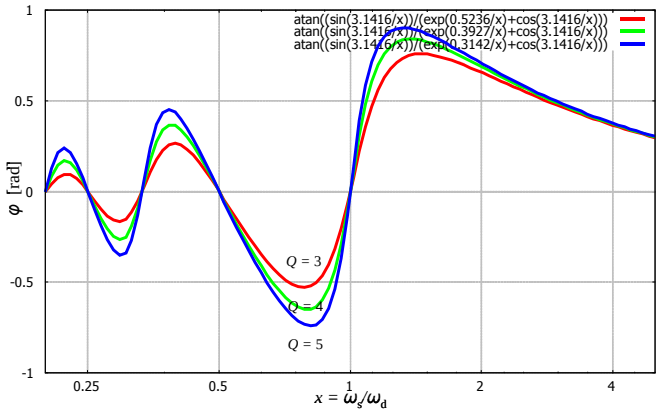

Fig. 5. Dependence of the phase angle φ on the normalized value ω_s/ω_d for Q = 3, 4 and 5, when excited by voltage pulses.

Also, the current waveform for $f_s = 0.5 \cdot f_d$ or $f_s = 0.6 \cdot f_d$ shows that it is very much distorted deep below resonance, the first harmonic is no longer dominant, which reflects to the amount of active power transferred to the load. This explains why below-resonance mode of power control was less desirable. The first diagram in Fig. 6 for $f_s = 0{,}5\ f_d$ shows that (7) gets zero values every time the switching period T_s is multiple of the damping one T_d, in this case $T_s = 2\ T_d$.

A comparison of the phase angle φ dependence on ω_s in both cases, with sinusoidal and pulse excitation, is given in Fig. 7. The switching angular frequency ω_s is normalized, in the first case with the resonant ω_0, and in the second with the damping angular frequency ω_d. The figure shows that there is a considerable difference, especially further away from the resonance point. However, making PSpice simulations and measuring the phase angle time equivalents t_φ, it was noticed that they have very close values in the above-resonance region as can be clearly seen in Fig. 8. Analyzing this fact lead us to a very interesting conclusion. Namely t_φ is calculated in a different way in both cases. When the circuit excitation is sinusoidal, the current is in the form:

$$i(t) = I_{max} \sin(\omega_s t - \varphi) = I_{max} \sin[\omega_s (t - t_\varphi)] \tag{18}$$

and

$$t_\varphi = \frac{\varphi}{\omega_s} = \varphi \frac{T_s}{2\pi} \tag{19}$$

In the second case with voltage pulses excitation, we have:

$$i(t) = I_{max} e^{-\alpha t} \sin(\omega_d t - \varphi) = I_{max} e^{-\alpha t} \sin[\omega_d (t - t_\varphi)] \tag{20}$$

and

$$t_\varphi = \frac{\varphi}{\omega_d} = \varphi \frac{T_d}{2\pi} \tag{21}$$

Relations (19) and (21) are similar, but profoundly different: ω_d and T_d are constants determined by the circuit parameters, while ω_s and T_s are variables that are changed by the control method and are used as x-axis in Figs. 7 and 8. This also shows that in the case with voltage pulses, the correct way to measure and calculate the phase angle is by using (21) which is not taken into account in many analysis and papers.

V. SQUARE PULSE EXCITATION POWER ANALYSIS

The active power at steady state can be obtained as:

$$P(T_s) = \frac{2}{T_S} \int_0^{\frac{T_s}{2}} V_{DC} i(t) \mathrm{d}t = V_{DC} I_{max} \frac{2}{T_S} \int_0^{\frac{T_s}{2}} e^{-\alpha t} \sin(\omega_d t - \varphi) \mathrm{d}t \tag{22}$$

This integral can be analytically solved as:

$$P(T_s) = -\frac{2 V_{DC} I_{max}}{T_S (\omega_d^{\ 2} + \alpha^2)} \{ e^{-\alpha t} [\alpha \sin(\omega_d t - \varphi) + \omega_d \cos(\omega_d t - \varphi)] \}_0^{\frac{T_s}{2}}$$

Using trigonometric transfiguration and (3) we obtain:

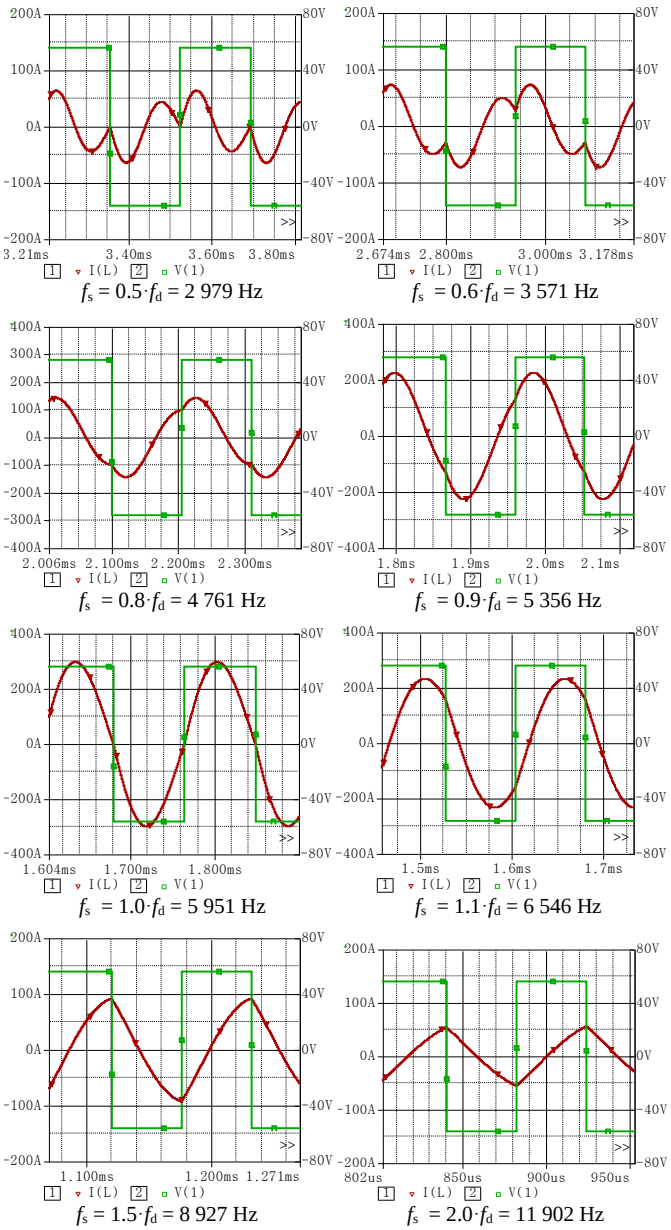

Fig. 6. Steady state voltage and current waveforms below and above resonance (R = 0.24 Ω, L = 26.5 μH, C = 26.6 μF and Q = 4).

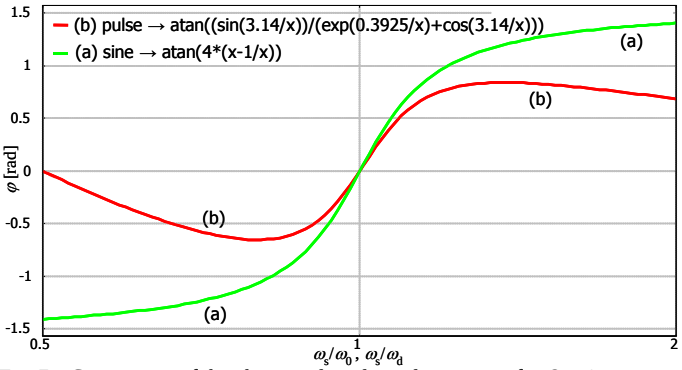

Fig. 7. Comparison of the phase angle φ dependence on ω_s for Q = 4: (a) sinusoidal excitation, $x = \omega_s/\omega_0$, (b) pulse excitation, $x = \omega_s/\omega_d$.

$$P(T_s) = -\frac{2 V_{DC} I_{max}}{\omega_0 T_S} \{ e^{-\alpha \frac{T_s}{2}} \sin[\omega_d \frac{T_s}{2} - \varphi + \arctan(\frac{\omega_d}{\alpha})] -$$

$$- \sin[-\varphi + \arctan(\frac{\omega_d}{\alpha})] \}$$

Introducing the normalized variable $x = \omega_s/\omega_d$ it has the form:

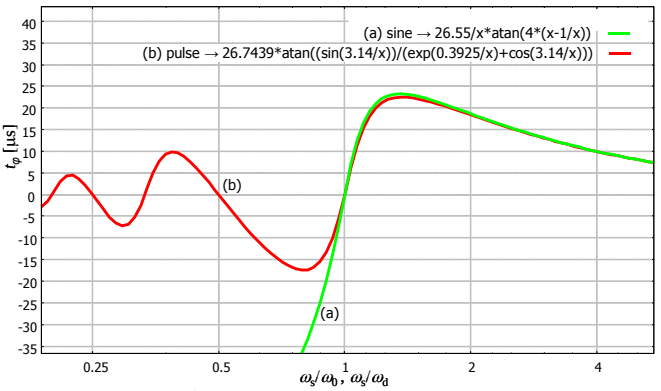

Fig. 8. Comparison of the phase angle time equivalent t_φ dependence on ω_s: (a) sinusoidal excitation, $x = \omega_s/\omega_0$, (b) pulse excitation, $x = \omega_s/\omega_d$.

$$P(x) = -\frac{2\omega_d V_{DC} I_{\max}}{\omega_0}\frac{x}{2\pi}\{e^{-\alpha\frac{\pi}{\omega_d x}}\sin[\frac{\pi}{x}-\varphi+\arctan(\frac{\omega_d}{\alpha})]-$$

$$-\sin[-\varphi+\arctan(\frac{\omega_d}{\alpha})]\}$$

Using (14) for $I_{\max}$ the for active power at steady state is:

$$P(x) = \frac{2\omega_d V_{DC}^{\ 2}}{\omega_0^{\ 2} L}\frac{x}{\pi}\frac{e^{-\frac{\alpha}{\omega_d}\frac{\pi}{x}}\sin[\frac{\pi}{x}-\varphi+\arctan(\frac{\omega_d}{\alpha})]-\sin[-\varphi+\arctan(\frac{\omega_d}{\alpha})]}{e^{-\frac{\alpha}{\omega_d}\frac{\pi}{x}}\sin[\frac{\pi}{x}-\varphi-\arctan(\frac{\omega_d}{\alpha})]+\sin[-\varphi-\arctan(\frac{\omega_d}{\alpha})]} \tag{23}$$

This relation is shown in Fig. 9 for the range of the normalized variable $x = \omega_s/\omega_d$ varied from one decade below to one decade above resonance ($x = 1$). The below resonance region is particularly interesting since it has unexpected behavior not reported in other analysis using harmonic waveforms decomposition. The active power P reduces to zero non monolithically with local maximums and minimums when the phase angle φ has values zero. The first such case when $\varphi = 0$ gives local power minimum is at $x = 0.5$ and corresponds to time waveforms in Fig. 6 for $f_s = 0.5 \cdot f_d$. This one, and other local minimums and maximums, correspond to ZCS (zero current switching) conditions and are of particular interest.

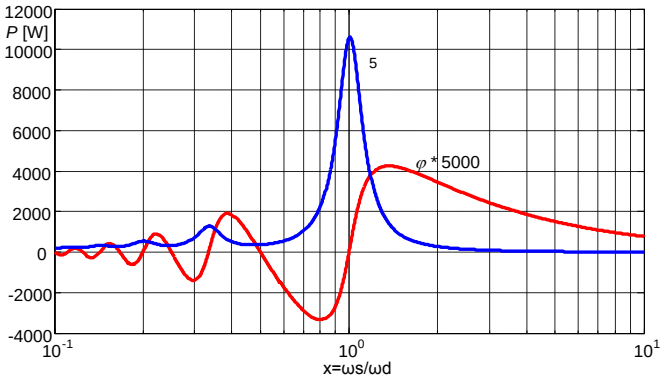

Fig. 9. Active power P dependence on switching frequency deviation from the damping frequency (blue line), phase angle φ (red line).

Figures 10, 11 and 12 show family of curves obtained when a certain resonant tank parameter is varied from its nominal value. This changes the quality factor of the resonant tank Q, and makes the power dependence oscillations below resonance stronger or weaker. Large portion of the power circulates between the source and the load in each half cycle. To measure it, we introduce "absolute" power defined as:

$$P_{\text{abs}}(x) = \frac{2}{T_S}\int_0^{\frac{T_s}{2}} V_{DD}|i(t)|\mathrm{d}t = V_{DD} I_{\max}\frac{3}{T_S}\int_0^{\frac{T_s}{2}} e^{-\alpha t}|\sin(\omega_d t-\varphi)|\mathrm{d}t \tag{24}$$

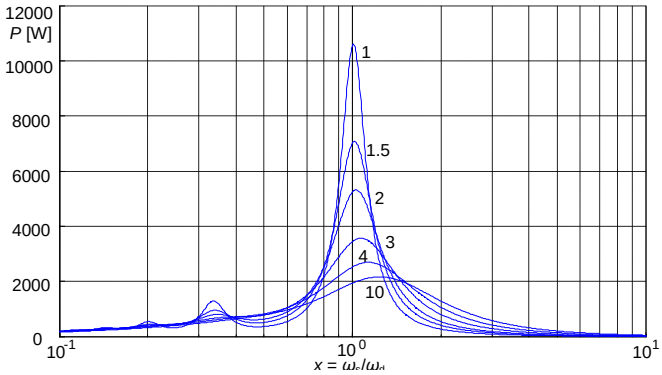

Fig. 10. Active power dependence on switching frequency deviation from the damping frequency. The family of curves are obtained varying the nominal resistance value R by a factor of k = 1; 1.5; 2; 3; 4 and 5.

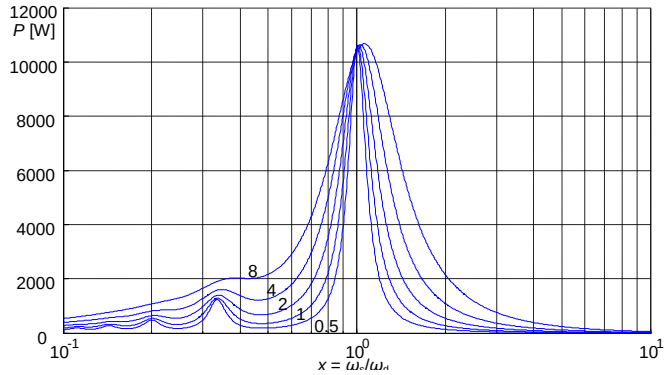

Fig. 11. Active power dependence on switching frequency deviation from the damping frequency. The family of curves are obtained varying the nominal capacitance value C by a factor of k = 0.5; 1; 2; 4; and 8.

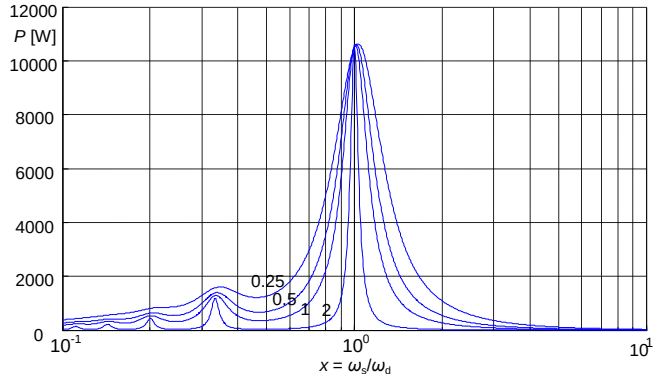

Fig. 12. Active power dependence on switching frequency deviation from the damping frequency. The family of curves are obtained varying the nominal inductance value L by a factor of k = 2; 1; 0.5; and 0.25.

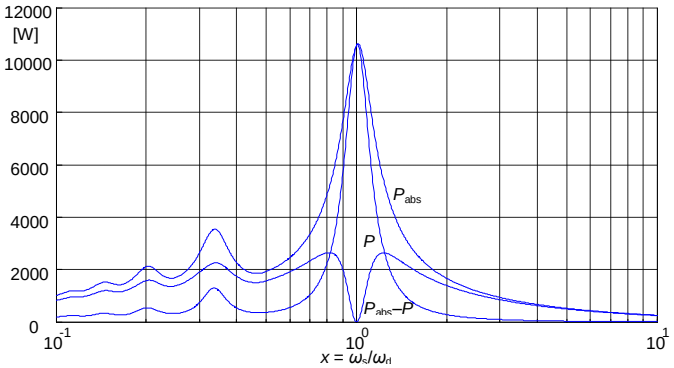

Fig. 13. Active power P, "absolute" power P_{abs}, and circulating power $P_{\text{abs}} - P$ dependence on switching frequency deviation from damping frequency at nominal values V_{DC} = 56 V, R = 0.24 Ω, L = 26.5 µH and C = 26.6 µF.

Figures 13 and 14 show this "absolute" power P_{abs}, as well as the difference P_{abs}–P that represents the circulating "reactive" power. The ratio P/P_{abs} has the meaning of the power factor.

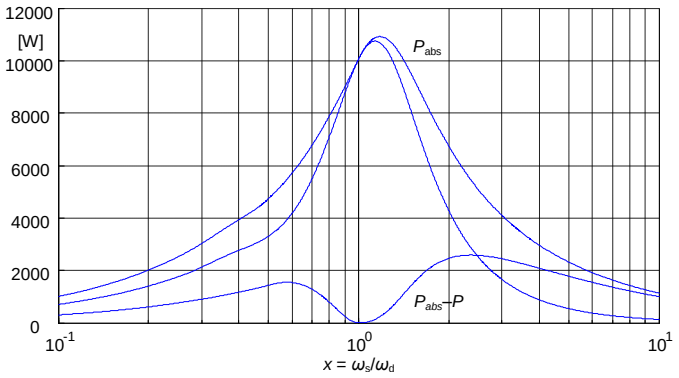

Fig. 14. Active power P, "absolute" power P_{abs}, and circulating power $P_{abs} - P$ dependence on switching frequency deviation from damping frequency with 16 times increased capacitance value $C = 16 \cdot 26.6\ \mu F = 425.6\ \mu F$.

Figures 15, 16 and 17 show the maximum values of the capacitance and inductance voltages and circuit current. These figures are useful in resonant tank elements design.

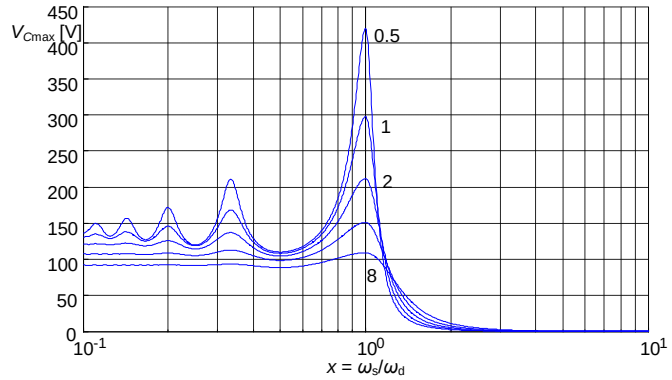

Fig. 15. Maximum capacitance voltage dependence on operating frequency deviation from damping frequency. The family of curves are obtained varying the nominal capacitance value C by a factor of k =0.5; 1; 2; 4; 8.

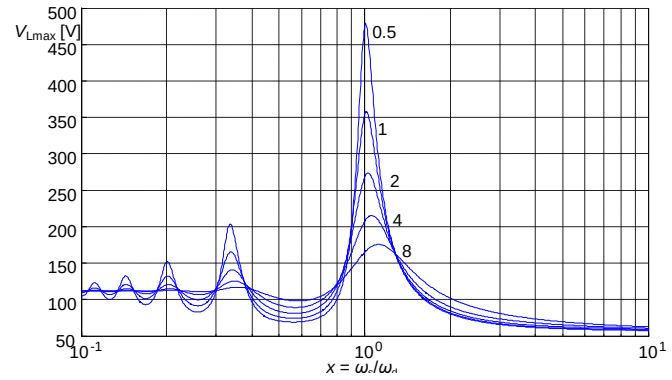

Fig. 16. Maximum inductance voltage dependence on operating frequency deviation from damping frequency. The family of curves are obtained varying the nominal capacitance value C by a factor of k = 0.5; 1; 2; 4; 8.

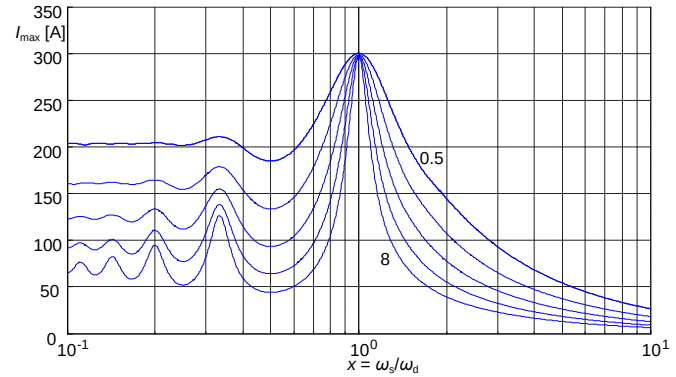

Fig. 17. Maximum circuit current I_{max} dependence on operating frequency deviation from damping frequency. The family of curves are obtained varying the nominal capacitance value C by a factor of k = 0.5; 1; 2; 4; 8.

VI. Conclusion

The derived analytical equations for the time variables, phase angle and power in the series resonant circuit excited by a square pulse voltage from a full-bridge converter are valid for the whole operating frequency range. Above resonance other approximate methods give satisfactory results. However, in the below resonance operation mode the current and voltage waveforms are very distorted and the analysis presented shows a considerably different dependence of the current phase angle and active power delivered to the load on the deviation of the switching frequency from the damping one. This new insight was not possible with other methods presented elsewhere. First, the phase angle in the case has to be calculated in respect to the damping frequency, which depends on circuit parameters, rather then in respect to the switching one, which is constantly varied by the control method. This fact is usually neglected in many analysis and papers. Second, the active power has peculiar osculating dependence with local maximums and minimums at zero phase angle below resonance. This can be used for ZCS if power is needed in defined steps. Derived equations allow for further investigations and optimisation, including the circuit power factor, depending on the circuit parameter values.

References

[1] Y. Deshmukh, Industrial Heating: Principles, Techniques, Materials, Applications and Design, Taylor and Francis Group, Boca Raton, 2005.

[2] V. Rudnev, D. Loveless, R. Cook, M. Black, Handbook of Induction Heating, Madison Heights, Michigan, USA, 2003.

[3] G. E. Totten, Steel Head Treatment, 2nd ed., Portland State University, Oregon USA, 2006.

[4] E. Rapoport, Y. Pleshitseva, Optimal Control of Induction Heating Processes, CRC Press, 2007.

[5] H. M. Unver, M. T. Aydemir, "Power and frequency control in a 60kW induction steel heating furnaces through PLC", National Scientific Meetings, Ankara, Turkey, 9–12 September 2002.

[6] Y. Kwon, S. Yoo, D. Hyun, "Half-bridge series resonant inverter for induction heating applications with load-adaptive PFM control strategy", Applied Power Electronics Conference and Exposition, pp. 575–581, Dallas, TX, USA, 14–18 Mar 1999.

[7] L. Grajales, F. C. Lee, "Control system design and small-signal analysis of a phase-shift-controlled series-resonant inverter for induction heating", Power Electronics Specialists Conference–PESC'95, Volume 1, pp. 450–456, 1995.

[8] W.-H. Ki, J. Shi, E. Yau, P. K. T. Mok, and J. K. O. Sin, "Phase controlled dimmable electronic ballast for fluorescent lamps," Power Electronics Specialists Conference–PESC'99, pp. 1121–1125, 1999.

[9] P. Viriya T. Thomas, "Power transfer characteristics of a phase-shift controlled ZVS inverter for the application of induction heating", Int. Power Electron. Conf.–IPEC, pp. 423–428, San Francisco, CA, 2000.

[10] Y. Yin, Z. Regan, "Digital phase control for resonant inverters", IEEE Power Electronics Letters, vol. 2, no. 2, pp. 51–54, June 2004.

[11] Y. Yin, M. Shirazi, R. Zane, "Electronic ballast control IC with digital phase control and lamp current regulation", IEEE Trans. Power Electron., vol. 23, no. 1, pp. 11 – 18, Jan 2008.

[12] F. J. Azcondo, R. Zane, and C. Branas, "Design of resonant inverters for optimal efficiency over lamp life in electronic ballast with phase control," IEEE Trans. Power Electron., vol. 22, no. 3, pp. 815–823, 2007.

[13] G. Stefanov, Lj. Karadzinov, "Phase controlled bridge converter with serial resonant load", 14th International Power Electronics and Motion Control Conference EPE-PEMC 2010, pp. T3 81–87, Ohrid, Macedonia, 6–8 Sep 2010.

[14] G. Stefanov, Lj. Karadzinov, T. Dzhekov, "Design of an IGBT bridge converter for serial resonant load", 14th International Power Electronics and Motion Control Conference, EPE-PEMC 2010, pp. T9 19–26, Ohrid, Macedonia, 6–8 Sep 2010.

[15] G. Stefanov, "Resonant Converter for Induction Heating of Metals with Improved Efficiency", Ph.D. Thesis, Sts. Cyril and Methodius University, Skopje, Macedonia, 2014.

[16] Lj. Karadzinov, G. Stefanov, "Direct phase digital control method in power inverters based on dumping frequency analysis", Proceedings of the 16-th IEEE International Conference on Computer as a Tool – IEEE EUROCON 2015, Salamanca, Spain, 8–11 Sep. 2015, pp. 1–6.